Dual-Junction GaAs Photovoltaics for Low Irradiance Wireless Power Transfer in Submillimeter-Scale Sensor Nodes

Eunseong Moon, *Member, IEEE*, Michael Barrow, *Student Member, IEEE*, Jongyup Lim, *Student Member, IEEE*, David Blaauw, *Fellow, IEEE*, and Jamie D. Phillips, *Senior Member, IEEE*

***Abstract*—Dual-junction GaAs photovoltaic (PV) cells and modules at submillimeter scale are demonstrated for efficient wireless power transfer for Internet of Things and bio-implantable applications under low-flux illumination. The dual-junction approach meets demanding requirements for these applications by increasing the output voltage per cell with reduced area losses from isolation and interconnects. A single PV cell (150 μm $\times$ 150 μm) based on the dual-junction design demonstrates power conversion efficiency above 22% with greater than 1.2 V output voltage under low-flux 850 nm near-infrared LED illumination at 6.62 μW/mm^2, which is sufficient for the batteryless operation of miniaturized CMOS IC chips. The output voltage of dual-junction PV modules with four series-connected cells demonstrates greater than 5 V for direct battery charging while maintaining a module power conversion efficiency of more than 23%.**

***Index Terms*—Bio-implants, Internet of Things (IoT), photovoltaic (PV) cells, wireless power transmission.**

I. Introduction

EFFICIENT wireless power transfer for millimeter scale or submillimeter-scale sensor systems [1]–[5] is a key technology, opens up new capabilities for the Internet of Tiny Things (IoT^2) [6], [7] and bio-implantable devices [8]–[10]. Photovoltaic (PV) power conversion [11]–[13] can be effective for harvesting ambient light efficiently from either solar irradiance or indoor lighting with above 20% power conversion efficiency for miniaturized IoT^2 sensors, and much greater efficiency than ambient radio frequency (RF) converters [8], [9] at these reduced dimensions. Near-infrared (NIR) light provides a means for high-power conversion efficiency (>30%) in millimeter-scale subcutaneous implantable devices [14]–[16], and overcomes limitations of RF energy harvesting at small scales because of low-antenna coupling efficiency [17]–[19] and/or loss at high frequency (>50 GHz) [8], [9]. Monochromatic PV power conversion, such as in laser power converters [20]–[24], has demonstrated high conversion efficiency (>50%) under high irradiance conditions (>100 mW/mm^2). Success for IoT^2 and bio-implantable devices requires high efficiency at substantially lower irradiance (<1 mW/mm^2) and at small cell dimensions, where PV performance becomes strongly impacted by loss mechanisms including shunt resistance and perimeter and surface recombination losses [15], [20].

In many of these millimeter-scale systems based on low-power CMOS chips [2]–[4], a minimum power requirement of these systems is around 50 nW/mm^2 [2], [13] for perpetual operation, which was supplied sufficiently using PV cells [11], [13]–[15] under low-flux conditions below 10 μW/mm^2. However, the output voltage must be upconverted to directly power CMOS circuitry (>1.2 V) [8] or for battery charging (>5 V) [7], [25] because of low output voltage of single PV cells below 1 V. Additional power management circuitry based on a switched capacitor network is required for dc–dc voltage up-conversion at small millimeter-scale dimensions, although there are inherently associated switching and conducting losses [26] limiting the overall power to roughly 50% of the original output power of PV cells. Series-connected single junction (SJ) PV modules at the millimeter scale have been demonstrated [26], [27], providing output voltage of greater than 5 V and voltage up-conversion efficiency of more than 90%. However, there are fill factor losses associated with shunt leakage paths through the shared substrate [20], [27], [28] and efficiency losses when scaling to small systems because of perimeter losses [15], [26]. There is a continuing challenge to miniaturize such PV systems down to the submillimeter scale with minimal optical losses from device isolation and metal interconnects and efficient voltage up-conversion. Vertically series-connected junctions offer an alternative option for efficient voltage up-conversion, which is commonly used for broadband solar illumination and devices with multiple junctions for differing bandgap energies [29]–[33]. Furthermore, vertical "segmented" multijunction (MJ) designs [21]–[24] based on up to 20 thin p-n GaAs junctions have been demonstrated under high NIR irradiance (>1.5 W/mm^2), generated an output voltage >20 V with power conversion efficiency

Manuscript received May 27, 2020; revised August 12, 2020; accepted September 16, 2020. Date of publication October 5, 2020; date of current version October 21, 2020. This work was supported by the National Institutes of Health under Award R21EY02945201. *(Corresponding author: Eunseong Moon.)*

Eunseong Moon, Michael Barrow, Jongyup Lim, and David Blaauw are with the Department of Electrical and Computer Engineering, University of Michigan, Ann Arbor, MI 48109 USA (e-mail: esmoon@umich.edu; barrowm@umich.edu; jongyup@umich.edu; blaauw@umich.edu).

Jamie D. Phillips was with the University of Michigan, Ann Arbor, MI 48109 USA. He is now with the Department of Electrical and Computer Engineering, University of Delaware, Newark, DE 19716 USA (e-mail: jphilli@udel.edu).

Color versions of one or more of the figures in this article are available online at https://ieeexplore.ieee.org.

Digital Object Identifier 10.1109/JPHOTOV.2020.3025450

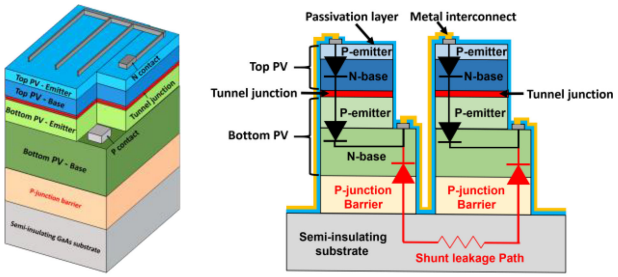

Fig. 1. Schematic diagrams of (a) single DJ PV cell and (b) DJ PV module illustrating PV cell junction, junction barrier isolation, and shunt leakage path.

above 60%. However, success in meeting specific requirements for low-flux applications and device miniaturization down to submillimeter scale has not been proven.

In this work, we demonstrate dual-junction (DJ) PV cells at submillimeter scale under low-flux illumination from NIR illumination to narrowband visible indoor lighting. The devices use junctions with the same GaAs-based materials and bandgap energies, where cells are designed to evenly divide optical absorption in each junction, while doubling the voltage output for the DJ series connection and considering demanding requirements for miniaturized devices under low-flux operating conditions. The DJ approach provides a means of voltage up-conversion while reducing the number of lateral series connections and corresponding shunt leakage paths for monolithic PV modules.

II. Dual Junction Device Design

Conventional MJ solar cells utilize monolithically grown [29]–[31] or mechanically stacked/bonded [32], [33] materials with optimized band gaps for differing spectral windows. The previous laser power converters [20]–[24] using vertically stacked multiple p-n GaAs junctions were designed for the NIR wavelength range between 800 and 850 nm. In this work, we design a monolithic DJ PV cell with GaAs absorber regions that are connected in series by a heavily doped tunnel junction, tunable both for visible indoor lighting and NIR LED illumination, operating extremely low-flux illumination conditions ($<10\ \mu$W/mm^2), miniaturized down to submillimeter scale using the optimized sidewall passivation studies, and stackable to the CMOS ICs directly [8]. The device structure concepts for single PV cell and module are shown in Fig. 1.

Photocurrent splitting for vertical MJs can be estimated by the following equation [33]:

$$G(x) = \int \alpha(E)\, b_s(E)\, e^{-\alpha(E)x} dE \tag{1}$$

where $G(x)$ is the photogeneration rate at thickness x, $b_s(E)$ is the incident photon flux at the surface of energy E (photons/unit area/s), and $\alpha(E)$ is the absorption coefficient. Thickness values for GaAs MJ designs at a wavelength of 850 nm with the total absorption above 99% are summarized in Table I, indicating that dual, triple, and quadruple junction approaches appear to have reasonable diode layer thicknesses, whereas the dual junction approach is the most convenient to control the thickness both for NIR and visible wavelength ranges.

TABLE I
Optimized Thickness of MJ Designs for a Wavelength of 850 nm

# of junctions	Thickness of Junction #1	Thickness of Junction #2	Thickness of Junction #3	Thickness of Junction #4
2	712 nm	3 µm		
3	412 nm	698 nm	3 µm	
4	296 nm	418 nm	715 nm	3 µm

TABLE II
Optimized Device Parameters of DJ PV Cell and Module, Designed for NIR Wavelength at 850 nm

Type	Material	Thickness (nm)	Doping (cm^{-3})	Layer information
P++	GaAs	200	$2x10^{19}$	anode
P+	$Al_{0.8}Ga_{0.2}As$	30	$2x10^{18}$	window
P+	GaAs	100	$4x10^{18}$	emitter
N	GaAs	500	$1x10^{17}$	base
N+	$Al_{0.3}Ga_{0.7}As$	30	$1x10^{18}$	BSF
N++	GaAs	15	$1x10^{19}$	TJ
P++	GaAs	15	$4x10^{19}$	TJ
P+	$Al_{0.8}Ga_{0.2}As$	30	$2x10^{18}$	window
P+	GaAs	500	$4x10^{18}$	emitter
N	GaAs	3000	$1x10^{17}$	base
N+	$Al_{0.3}Ga_{0.7}As$	150	$1x10^{18}$	BSF
N++	GaAs	1000	$2x10^{18}$	cathode
P-	$Al_{0.3}Ga_{0.7}As$	400	$5x10^{16}$	barrier
--	GaAs		Semi-insulating	substrate

Detailed device parameters for DJ cells were optimized for 850 nm wavelength utilizing Sentaurus Device [35] and physical models for band-to-band tunneling, drift-diffusion currents, and photocurrent generation. The design is based on prior SJ cells [15], [27] incorporating window layers and back surface field, with details shown in Table II. An additional $Al_{0.3}Ga_{0.7}As$ layer is incorporated between the bottom cell and substrate to serve as a junction barrier to reduce shunt leakage for monolithic series-connected modules [27].

The simulated external quantum efficiency (EQE) demonstrates a maximum response at a particular wavelength (see Fig. 2) corresponding to the current matched condition for the two cells. We can control the EQE peak wavelength by defining the total thickness of the top cell, ranging from approximately 600 nm for a 100 nm thick top junction to 850 nm for a 600 nm thick top junction. While similar peak EQE above 40% is attained for all these different top junction thicknesses, the conversion efficiencies vary considerably because of thermalization losses for photon energies further away from the material bandgap.

Electrical power conversion is illustrated by the simulated current density versus voltage (J–V) characteristics of DJ PV cells in Fig. 3(a), comparing to SJ PV cells with similar total thickness under low-flux 850 nm NIR illumination. For

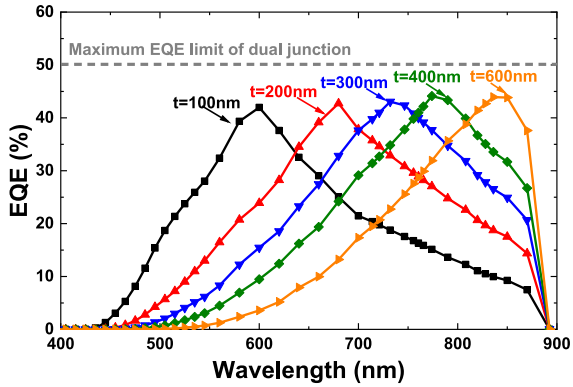

Fig. 2. Simulated EQE spectra for different thickness of top PV cells in the DJ structure with the fixed thickness of bottom PV cell at 3.5 μm.

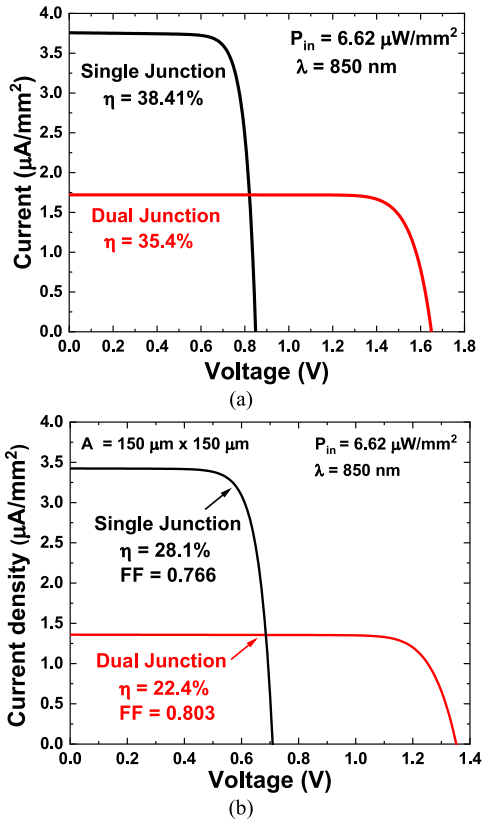

Fig. 3. Comparison of (a) simulated and (b) measured *J–V* characteristics between DJ and SJ PV cells under 850 nm NIR illumination at 6.62 μW/mm^2.

reference, the incident flux of 1 μW/mm^2 is approximately 1000 times lower than one-sun solar irradiation (1 mW/mm^2 [36]) and is similar to typical indoor lighting conditions of around 400 lux [11]. The simulated *J–V* results for DJ cells under NIR illumination shown in Fig. 3(a) demonstrate that optimized DJ PV cells have a comparable power conversion efficiency (>30%) to SJ PV cells with a doubling of the output voltage (>1.4 V).

III. Device Fabrication and Testing Methods

Wafers based on optimized layer structures (see Table II) from the simulation were grown by molecular beam epitaxy on semi-insulating GaAs substates. We fabricated square DJ PV

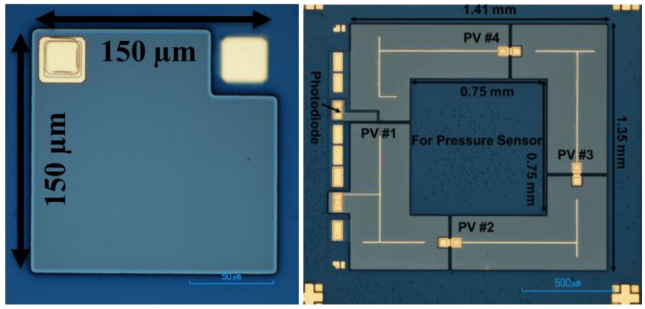

Fig. 4. Optical microscope images of (a) fabricated DJ PV cell at μm scale and (b) DJ PV module that have four cells connected in series.

cells ranging from 100 μm to 2.5 mm on a side. Devices were fabricated using conventional photolithography, etching, contact metallization, and liftoff processes, as shown in Fig. 4(a). Special attention was devoted to surface/perimeter passivation because of their importance for miniaturized PV cell performance [14], [15], [37], where we used a diluted ammonium sulfide solution treatment [15] for 3 min to etch the native oxide and passivate broken bonds on the sidewall using the additional sulfur bonds and a subsequent 100 nm plasma-enhanced chemical vapor deposition silicon nitride passivation layer that also serves as a top surface antireflection coating with the measured reflectance below 5% at a wavelength of 850 nm. Monolithic PV cell modules were fabricated with four and eight connected cells in series using lithographically defined metal interconnects, as shown in Fig. 4(b). These monolithic DJ modules provide voltage upconversion that combines both vertical and lateral series connections. Electrical characteristics (*J–V* and *P–V*) under NIR illumination conditions were measured using a Keithley 4200/2400 parameter analyzer. NIR illumination up to 10 μW/mm^2 used a commercial 850 nm NIR light-emitting diode and calibrated power meter. The EQE spectrum was measured using a grating monochromator, xenon white light source, lock-in amplifier, and calibrated photodetector. The measured *J–V* and power density versus voltage (*P–V*) characteristics were used to extract $J_{\rm SC}$, open-circuit voltage ($V_{\rm OC}$), maximum power density ($P_{\rm max}$), and fill factor FF $= P_{\rm max}/(V_{\rm OC} * J_{\rm SC})$.

IV. Results

The device performance of DJ cells under 850 nm illumination is shown in Fig. 3(b) and compared with SJ PV cells. The DJ cells demonstrate a near doubling of output voltage (>1.2 V) and approximately 40% of the current relative to the SJ case. The DJ device demonstrates a high fill factor near 80%, indicating that shunt resistance is not problematic. The power conversion efficiency decreases from 28.1% for the SJ case to 22.4% for the DJ case. The source of reduced photo-generated current may be examined by the EQE spectra shown in Fig. 5. The peak EQE response of the DJ PV cell is close to an 860 nm wavelength that is slightly longer than a desired 850 nm wavelength, indicating a thicker upper cell than the optimized parameters in Table I. Furthermore, the measured peak EQE for the DJ decreases to 38% from the simulated value of 45%, corresponding to the observed reduction in current density in comparison to the SJ

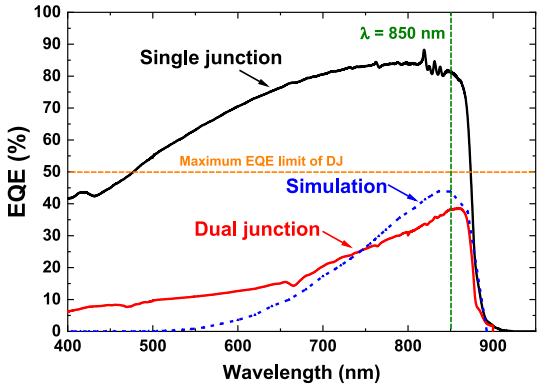

Fig. 5. Measured EQE spectra of DJ and SJ PV cells and comparison with simulated EQE spectrum of DJ PV cell.

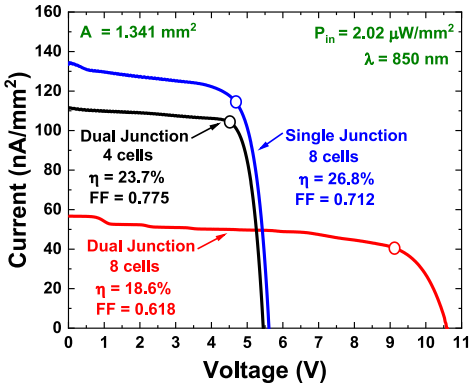

Fig. 6. Comparison of measured *J–V* characteristics between SJ PV arrays (eight cells in series) and DJ PV arrays using four cells and eight cells in series under 850 nm NIR illumination at 2.02 μW/mm^2 with maximum power points.

cell. The source of this current reduction may be associated with a parasitic absorption in the 30 nm tunnel junction around 3%–4% in the NIR range between 800 and 850 nm and/or nonideal behavior of the tunnel junction at the relatively low current densities examined in this study.

Power conversion in monolithic PV modules with four and eight series-connected DJ cells is shown in Fig. 6, demonstrating higher output voltage that is suitable for direct battery charging capabilities. PV modules with four series-connected DJ cells (total of eight diode junctions) produce an output voltage >5 V, power conversion efficiency of 23.7%, and overall voltage up-conversion efficiency of approximately 84% compared with baseline SJ PV cells with the output voltage below 1 V. The eight series-connected DJ cell module (total of 16 series-connected diode junctions) produces an output voltage >10 V with an efficiency of more than 18%, where there is a clear drop in fill factor because of the shunt leakage degradation [20], [28].

V. Discussion

The performance of SJ and DJ PV modules under 850 nm NIR illumination is compared in Fig. 6. PV modules targeted for >5 V operation use either four series-connected DJ cells or eight series-connected SJ cells, where the DJ PV module shows an improved FF = 0.775 in comparison to the SJ PV module

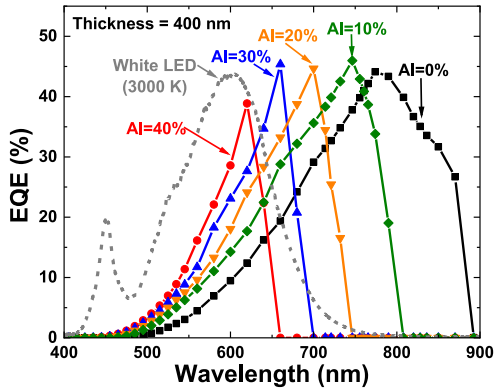

Fig. 7. Simulated EQE spectra for variable aluminum mole fraction of top PV cells in the DJ structure with the fixed thickness of top PV cell at 400 nm and comparison with the normalized spectrum of commercialized white LED with 3000 K color temperature.

with FF = 0.712 by reducing the shunt leakage paths between series-connected PV cells through the substrate. However, the power conversion efficiency of the DJ PV module is degraded from 26.8% to 23.7% because of the photo-generated current reduction from the parasitic absorption in the tunnel junction for individual DJ PV cells. Although there was the performance degradation especially in the fill factor for the DJ PV modules because of shunt leakage current over the junction barrier, main advantages of the DJ epitaxial structure with lateral series connections compared with all vertically stacked MJ structures are to control the peak wavelength from visible to NIR ranges conveniently by optimizing the thickness of the upper cell as shown in Fig. 2 and to reduce the optical losses from the parasitic absorption in multiple tunnel junctions.

The data thus far have focused on a wavelength of 850 nm, providing an important spectral region for either bio-implantable devices or laser power converters. Extending the DJ approach to indoor lighting applications requires designs that shift the peak EQE toward visible wavelengths. This may be accomplished by either reducing the top junction thickness (see Fig. 2), or increasing the bandgap energy for the optical absorption regions of the device. Reducing the thickness of a top GaAs junction is not an optimal solution since the bandgap energy of GaAs material at 1.424 eV is not perfectly adequate for the indoor lighting spectrum [11], [38], requiring wider bandgap around 1.9 eV. Increasing aluminum content in the top GaAs absorbing region can be an effective approach to shift peak EQE to the visible spectral region while also maintaining practical thickness values for the top junction. Simulated EQE spectra for DJ designs with varying aluminum mole fraction in top junctions are shown in Fig. 7, demonstrating a shift to visible wavelengths. High EQE values are reached in the 600–650 nm region, corresponding to high flux regions for the soft white artificial lighting with 3000 K color temperature. Simulated *J–V* characteristics for DJ designs with GaAs and $Al_{0.4}Ga_{0.6}As$ absorber top junctions are shown in Fig. 8 for illumination with a soft white LED. The use of higher aluminum mole fraction in the top cell results in a substantial increase in power conversion efficiency with values exceeding 30%. The incorporation of a wider bandgap

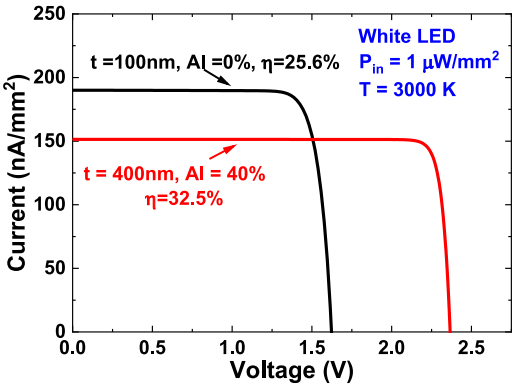

Fig. 8. Simulated *J*–*V* characteristics of DJ cells with variable aluminum mole fraction of a top cell under white LED illumination (3000 K color temperature) at 1 μW/mm^2.

top junction also provides a higher output voltage because of the more optimal match to the ideal bandgap energy for the indoor lighting spectrum [11], [38].

Further improvements in the performance of DJ PV cells and modules are possible from further optimization of the tunnel junction and layer structure of the top junction to reduce photo-generated current losses. The shunt leakage current of PV modules through the substrate can be reduced using thicker junction barrier layers with wider bandgap AlGaAs (>30% aluminum) or techniques such as epitaxial lift-off [31], [39] and microtransfer printing [40] to transfer the active layers to insulating substates or vertically stacked MJ designs [23] rather than laterally interconnected cells.

VI. Conclusion

Vertically stacked DJ PV cells and modules are demonstrated to increase operating voltage for direct powering of miniature devices for Internet of Things and bio-implantable applications with low-irradiance narrowband spectral illumination. The DJ approach increases the output voltage per cell and minimizes area losses from device isolation and interconnects in comparison to SJ cells. DJ PV cells at small dimensions (150 μm $\times$ 150 μm) demonstrate power conversion efficiency greater than 22% with more than 1.2 V output voltage under low-flux 850 nm NIR LED illumination at 6.62 μW/mm^2, which is sufficient for the batteryless operation of miniaturized CMOS IC chips. The output voltage of DJ PV modules with four series-connected single cells was greater than 5 V while maintaining an efficiency of more than 23%. Further power conversion efficiency improvements are expected by optimizing designs to minimize photocurrent collection losses and shunt resistance losses through the substrate in modules. In addition to NIR illumination, the GaAs DJ approach also shows promise for efficient energy harvesting under narrowband artificial indoor lighting conditions.

Acknowledgment

The content is solely the responsibility of the authors and does not necessarily represent the official views of the National Institutes of Health.

References

[1] B. Warneke, M. Last, B. Liebowitz, and K. S. J. Pister, "Smart dust: Communicating with a cubic-millimeter computer," *Computer*, vol. 34, no. 1, pp. 44–51, 2001.

[2] Y. Lee *et al.*, "A modular 1 mm^3 die-stacked sensing platform with low power I^{2}C inter-die communication and multi-modal energy harvesting," *IEEE J. Solid-State Circuits*, vol. 48, no. 1, pp. 229–243, Jan. 2013.

[3] G. Kim *et al.*, "A millimeter-scale wireless imaging system with continuous motion detection and energy harvesting," in *Proc. IEEE Symp. VLSI Circuits Dig. Techn. Papers*, 2014, pp. 1–2.

[4] T. Jang *et al.*, "Millimeter-scale computing platform for next generation of Internet of Things," in *Proc. IEEE Int. Conf. RFID*, 2016, pp. 1–4.

[5] J. S. Pulskamp, G. P. Ronald, and K. Oldham, "Highly integrated PiezoMEMS enabled millimeter-scale robotics," in *Proc. ASME Int. Des. Eng. Tech. Conf. Comput. Inf. Eng. Conf.*, 2009, pp. 797–805.

[6] S. Oh *et al.*, "IoT^2—The Internet of Tiny Things: Realizing mm-scale sensors through 3D die stacking," in *Proc. IEEE Des., Autom. Test Eur. Conf. Exhib.*, 2019, pp. 686–691.

[7] I. Lee, E. Moon, Y. Kim, J. Phillips, and D. Blaauw, "A 10mm^3 light-dose sensing IoT^2 system with 35-to-339 nW 10-to-300 klx light-dose-to-digital converter," in *Proc. IEEE Symp. VLSI Technol.*, 2019, pp. C180–C181.

[8] J. Lim *et al.*, "26.9 A 0.19$\times$ 0.17 mm^2 wireless neural recording IC for motor prediction with near-infrared-based power and data telemetry," in *Proc. IEEE Int. Solid-State Circuits Conf.*, 2020, pp. 416–418.

[9] J. Lee *et al.*, "Wireless power and data link for ensembles of sub-mm scale implantable sensors near 1GHz," in *Proc. IEEE Biomed. Circuits Syst. Conf.*, 2018, pp. 1–4.

[10] S. Lee *et al.*, "A 250 μm$\times$ 57 μm microscale opto-electronically transduced electrodes (MOTEs) for neural recording," *IEEE Trans. Biomed. Circuits Syst.*, vol. 12, no. 6, pp. 1256–1266, Dec. 2018.

[11] A. S. Teran *et al.*, "AlGaAs photovoltaics for indoor energy harvesting in mm-scale wireless sensor nodes," *IEEE Trans. Electron Devices*, vol. 62, no. 7, pp. 2170–2175, Jul. 2015.

[12] I. Mathews, P. J. King, F. Stafford, and R. Frizzell, "Performance of III–V solar cells as indoor light energy harvesters," *IEEE J. Photovolt.*, vol. 6, no. 1, pp. 230–235, Jan. 2016.

[13] A. S. Teran *et al.*, "Energy harvesting for GaAs photovoltaics under low-flux indoor lighting conditions," *IEEE Trans. Electron Devices*, vol. 63, no. 7, pp. 2820–2825, Jul. 2016.

[14] E. Moon, D. Blaauw, and J. D. Phillips, "Subcutaneous photovoltaic infrared energy harvesting for bio-implantable devices," *IEEE Trans. Electron Devices*, vol. 64, no. 5, pp. 2432–2437, May 2017.

[15] E. Moon, D. Blaauw, and J. D. Phillips, "Infrared energy harvesting in millimeter-scale GaAs photovoltaics," *IEEE Trans. Electron Devices*, vol. 64, no. 11, pp. 4554–4560, Nov. 2017.

[16] K. Song *et al.*, "Subdermal flexible solar cell arrays for powering medical electronic implants," *Adv. Healthcare Mater.*, vol. 5, no. 13, pp. 1572–1580, 2016.

[17] R.-F. Xue, K.-W. Cheng, and M. Je, "High-efficiency wireless power transfer for biomedical implants by optimal resonant load transformation," *IEEE Trans. Circuits Syst. I, Reg. Papers*, vol. 60, no. 4, pp. 867–874, Apr. 2013.

[18] A. K. RamRakhyani, S. Mirabbasi, and M. Chiao, "Design and optimization of resonance-based efficient wireless power delivery systems for biomedical implants," *IEEE Trans. Biomed. Circuits Syst.*, vol. 5, no. 1, pp. 48–63, Feb. 2011.

[19] M. Catrysse, B. Hermans, and R. Puers, "An inductive power system with integrated bi-directional data-transmission," *Sensors Actuators A, Phys.*, vol. 115, nos. 2/3, pp. 221–229, Sep. 2004.

[20] R. Kimovec, H. Helmers, A. W. Bett, and M. Topič, "Comprehensive electrical loss analysis of monolithic interconnected multi-segment laser power converters," *Prog. Photovolt., Res. Appl.*, vol. 27, pp. 199–209, 2019.

[21] S. Fafard *et al.*, "High-photovoltage GaAs vertical epitaxial monolithic heterostructures with 20 thin p/n junctions and a conversion efficiency of 60%," *Appl. Phys. Lett.*, vol. 109, no. 13, 2016, Art. no. 131107.

[22] S. Fafard *et al.*, "Ultrahigh efficiencies in vertical epitaxial heterostructure architectures," *Appl. Phys. Lett.*, vol. 108, no. 7, 2016, Art. no. 071101.

[23] Y. Zhao, Y. Sun, Y. He, S. Yu, and J. Dong, "Design and fabrication of six-volt vertically-stacked GaAs photovoltaic power converter," *Sci. Rep.*, vol. 6, no. 1, 2016, Art. no. 38044.

[24] D. Krut *et al.*, "Monolithic multi-cell GaAs laser power converter with very high current density," in *Proc. Conf. Rec. 29th IEEE Photovolt. Spec. Conf.*, 2002, pp. 908–911.

[25] I. Lee *et al.*, "A 179-lux energy-autonomous fully-encapsulated 17-mm^3 sensor node with initial charge delay circuit for battery protection," in *Proc. IEEE Symp. VLSI Circuits*, 2018, pp. 251–252.
[26] I. Lee *et al.*, "21.4 A>78%-efficient light harvester over 100-to-100klux with reconfigurable PV-cell network and MPPT circuit," in *Proc. IEEE Int. Solid-State Circuits Conf.*, 2016, pp. 370–371.
[27] E. Moon, I. Lee, D. Blaauw, and J. D. Phillips, "High-efficiency photovoltaic modules on a chip for millimeter-scale energy harvesting," *Prog. Photovolt., Res. Appl.*, vol. 27, no. 6, pp. 540–546, 2019.
[28] R. Pena and C. Algora, "The influence of monolithic series connection on the efficiency of GaAs photovoltaic converters for monochromatic illumination," *IEEE Trans. Electron Devices*, vol. 48, no. 2, pp. 196–203, Feb. 2001.
[29] K. Sasaki *et al.*, "Development of InGaP/GaAs/InGaAs inverted triple junction concentrator solar cells," *AIP Conf. Proc.*, vol. 1556, no. 1, pp. 22–25, 2013.
[30] J. F. Geisz *et al.*, "40.8% efficient inverted triple-junction solar cell with two independently metamorphic junctions," *Appl. Phys. Lett.*, vol. 93, no. 12, 2008, Art. no. 123505.
[31] R. Tatavarti *et al.*, "InGaP/GaAs/InGaAs inverted metamorphic (IMM) solar cells on 4″ epitaxial lifted off (ELO) wafers," in *Proc. 35th IEEE Photovolt. Spec. Conf.*, 2010, pp. 2125–2128.
[32] S. Essig *et al.*, "Raising the one-sun conversion efficiency of III–V/Si solar cells to 32.8% for two junctions and 35.9% for three junctions," *Nature Energy*, vol. 2, no. 9, 2017, Art. no. 17144.
[33] R. Cariou *et al.*, "III–V-on-silicon solar cells reaching 33% photoconversion efficiency in two-terminal configuration," *Nature Energy*, vol. 3, no. 4, pp. 326–333, 2018.
[34] G. Verzellesi, M. C. Vecchi, M. Zen, and M. Rudan, "Optical generation in semiconductor device analysis—A general purpose implementation," in *Proc. 4th Int. Conf. Simul. Semicond. Devices Processes*, 1991, pp. 57–64.
[35] Sentaurus Device User Guide, E. Version, Synopsys Inc., Mountain View, CA, USA, 2013.
[36] C. Riordan and R. Hulstron, "What is an air mass 1.5 spectrum? (Solar cell performance calculations)," in *Proc. IEEE Conf. Photovolt. Spec.*, 1990, pp. 1085–1088.
[37] E. Moon, D. Blaauw, and J. D. Phillips, "Small-area Si photovoltaics for low-flux infrared energy harvesting," *IEEE Trans. Electron Devices*, vol. 64, no. 1, pp. 15–20, Jan. 2017.
[38] M. Freunek, M. Freunek, and L. M. Reindl, "Maximum efficiencies of indoor photovoltaic devices," *IEEE J. Photovolt.*, vol. 3, no. 1, pp. 59–64, Jan. 2013.
[39] K. Lee, J. D. Zimmerman, T. W. Hughes, and S. R. Forrest, "Nondestructive wafer recycling for low-cost thin-film flexible optoelectronics," *Adv. Funct. Mater.*, vol. 24, no. 27, pp. 4284–4291, 2014.
[40] I. Mathews *et al.*, "Microtransfer printing high-efficiency GaAs photovoltaic cells onto silicon for wireless power applications," *Adv. Mater. Technol.*, vol. 5, 2020, Art. no. 2000048.